THE UNIVERSITY OF MICHIGAN

DEPARTMENT OF ELECTRICAL ENGINEERING
COOLEY ELECTRONICS LABORATORY

Technical Report No. 106

A Study of Traveling-Wave Directional Filters with Wideband Ferrite Tuning

By: D. K. ADAMS

Approved by: A. B. MACNEE

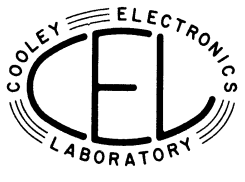

Under Contract With :

CONTRACT NO. DA-36-039 sc-78283, DEPT. OF ARMY
PROJ. NO. 3A99-06-001-01, PLACED BY: U. S. ARMY
SIGNAL RESEARCH AND DEVELOPMENT LABORATORY,
FORT MONMOUTH, N. J.

April 1961

THE UNIVERSITY OF MICHIGAN RESEARCH INSTITUTE • ANN ARBOR

ERRATA

Page 15, Eq. 29 should read:

$$\frac{(k_a r_1)J_m'(k_a r_1)}{J_m(k_a r_1)} = \frac{1}{\mu_e}\left[\frac{(k_f r_1)J_m(k_f r_1)}{J_m(k_f r_1)} + \frac{2J_m(k_f b)}{\pi J_m(k_f r_1)\left[J_m(k_f b)N_m(k_f r_1) - J_m(k_f r_1)N_m(k_f b)\right]} \pm m\not{\psi}\right] \qquad (29)$$

Page 16, Eq. 30 should read:

$$\frac{1}{\mu \mp \nu} \qquad (30)$$

Page 16, Eq. 31 should read:

$$\frac{1}{\mu \mp \nu} + \frac{1}{\mu_e}\left(\frac{2b^2}{r_1^2 - b^2}\right) \qquad (31)$$

Page 16, line 15 should read:

vs. r_2 and $(b - r_1)$ (i.e., the post radius and ring thickness, respectively) when the

Page 18, Eq. 33 should read:

$$J_1(k_a r_1) = 0 \qquad (33)$$

Page 18, line 10 should read:

radius r_2. Thus - - - - - - - -

THE UNIVERSITY OF MICHIGAN
OFFICE OF RESEARCH ADMINISTRATION
ANN ARBOR

A STUDY OF TRAVELING-WAVE DIRECTIONAL FILTERS WITH WIDEBAND FERRITE TUNING

Technical Report No. 106

2899-22-T

Cooley Electronics Laboratory
Department of Electrical Engineering

By: D. K. Adams (David Kendall)

Approved by: A. B. Macnee

Project 2899

TASK ORDER NO. EDG-4
CONTRACT NO. DA-36-039 sc-78283
SIGNAL CORPS, DEPARTMENT OF THE ARMY
DEPARTMENT OF ARMY PROJECT NO. 3A99-06-001-01

April 1961

TABLE OF CONTENTS

LIST OF ILLUSTRATIONS

LIST OF SYMBOLS

S_{ij}	General scattering matrix coefficient
a_j	Incident signal at port j of network
b_i	Emerging signal at port j of network
H	General tuning parameter
F(f)	Transmission amplitude characteristic for tunable filter
$\sin^2\theta_n$	Power coupling coefficient for nth directional coupler
φ_p	Complex phase shift in traversing path of L_p
α	Dissipative component of propagation constant in filter
β	Phase component of propagation constant in filter
H_r, H_φ, H_z	Components of RF magnetic field in r, φ, and z directions
E_r, E_φ, E_z	Components of RF electric field in r, φ, and z directions
r, φ, z	Polar coordinates
m, n, p	Indices of normal modes in geometry with cylindrical symmetry
h	Height of coaxial cavity
ω	Angular frequency of EM wave
k_c	Guide wave number $\left(\frac{2\pi}{\lambda g}\right)$ for propagation in a coaxial waveguide
μ_o, ϵ_o	Permeability and dielectric constant in free space
ϵ_r	Dielectric constant relative to free space
$J_m(x)$, $N_m(x)$	mth order Bessel functions of first and second kind
$C_m(x)$	Linear combination of $J_m(x)$ and $N_m(x)$
a,b	Inner and outer radii of coaxial cavity
$\|\|\mu\|\|$	Polder tensor representing permeability of saturated ferrite

LIST OF SYMBOLS (Continued)

μ, ν	Components of Polder tensor
μ_e	Effective permeability of ferrite (see Eq. 21)
ψ	ν/μ (see Eq. 21)
k_f, k_a	Wave numbers in homogeneous media of ferrite or air (see Eq. 21).
J_γ, N_γ	Bessel functions of (complex) order γ of first and second kind
X_γ, Z_γ	Particular linear combinations of J_γ and N_γ
I_γ, K_γ	Modified Bessel functions of first and second kinds
r_1, r_2	Inner and outer radii of ferrite ring in coaxial cavity
H_o	DC magnetic field used for tuning
H_{or}	Value of H_o corresponding to ferromagnetic resonance
M_o	Saturation magnetization of ferrite

ABSTRACT

Consideration is given to the possibility of employing ferrite for wideband frequency tuning in a class of narrowband, reflectionless filters employing traveling-wave resonators. Theoretical arguments are presented for choosing a symmetrically loaded cylindrical resonator, operating in the unloaded TM_{110} mode, as the tunable resonator for this filter. Exact, but implicit, expressions are formulated for the resonant frequencies and field configurations in this ferrite-loaded resonator for all $TM_{m,n,o}$ modes.

For the cases where the ferrite geometry is a post at the center of the resonator or a ring on the outer wall of the resonator, and when ferrite losses are negligible, the previous expressions are reduced to a more convenient form. When the ferrite is unmagnetized, a numerical solution is given for the resonant frequencies of the TM_{110} and TM_{210} modes. When the effective ferrite permeability (μ_e) is zero, the resonant frequency of the TM_{110} mode is similarly found. These three frequencies have been used to estimate the useful tuning range of this filter, as a function of the ferrite dimensions, for both ferrite configurations.

An experimental model of this filter has been constructed using the ring geometry. This device had a tuning envelope with less than 10 db insertion loss and more than 20 percent bandwidth at X-band. Suggestions are given regarding possible methods of improving these values, particularly the rather high insertion loss.

A STUDY OF TRAVELING-WAVE DIRECTIONAL FILTERS WITH WIDEBAND FERRITE TUNING

1. INTRODUCTION

During the past few years ferrite materials have been used for both wideband tuning (> 20 percent) of conventional cavities (Refs. 1, 2) and narrowband tuning (< 10 percent) of reflectionless resonant filters (Refs. 3, 4). However, a great many potential applications for tunable microwave filters require both wide tuning ranges and matched terminal conditions. The problem considered here is that of tuning narrowband filter characteristics over a wide frequency range. Specifically, the characteristics of interest are those of the four-port, reflectionless, narrowband, directional filter represented schematically in Fig. 1. In scattering matrix notation, this ideal filter has the following description.

$$b_i = \sum_{j=1}^{4} S_{ij} a_j; \qquad i = 1, 2, 3, 4 \tag{1a}$$

$$S_{ii} = 0 \tag{1b}$$

$$|S_{31}|^2 = |S_{24}|^2 = F[f - f_o(H)] \tag{1c}$$

$$|S_{21}|^2 = |S_{34}|^2 = 1 - F[f - f_o(H)] \tag{1d}$$

Here, a_j is the incident signal at port j, b_i is the emerging signal at port i, $F[f - f_o(H)]$ is assumed to be a narrow, bandpass characteristic such as that sketched in Fig. 1, and H is a tuning parameter. When ferrite tuning is employed, H represents an externally applied magnetic field. In this case, the anisotropic nature of ferrite may cause the scattering matrix to be unsymmetrical. Therefore, the following definitions of the remaining scattering matrix elements are generally consistent

with those in Eq. 1.

$$|S_{13}|^2 = |S_{42}|^2 = F[f - f_o'(H)] \tag{2a}$$

$$|S_{12}|^2 = |S_{43}|^2 = F[f - f_o'(H)] \tag{2b}$$

It is further assumed to be desirable that f_o and f_o' be linear, single-valued functions of H. For a reciprocal filter, $f_o' = f_o$.

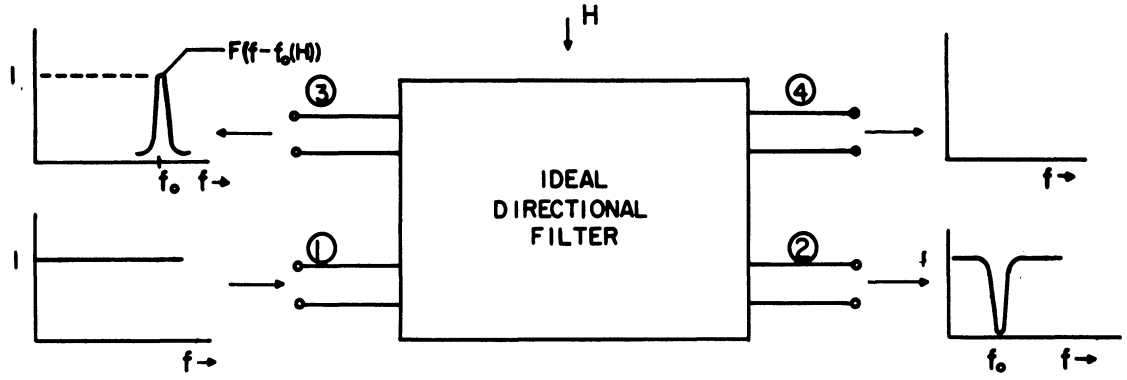

Fig. 1. Desired output spectral distributions with uniform incident spectrum at port (1).

While considerable effort has gone into the development of ferrite tunable circuits to approximate the characteristics specified above, the results to date have compromised these anticipated goals. Although large tuning ranges have been obtained, difficulty has been encountered in obtaining a satisfactory insertion loss between arms 1 and 3 over a large tuning range. This limitation on filter transmission can be attributed primarily to losses in the ferrite. In the filter structures to be described, other mechanisms can contribute heavily to insertion loss, but in principle these can be made quite small by careful design of the metallic portions of the filter. The purpose of this report then is to summarize: (1) design considerations that have been employed in this problem, (2) experimental results obtained to date,

and (3) theoretical considerations that could lead to improved versions of this filter.

2. DISCUSSION OF COUPLING NETWORKS

A basic circuit by which the above filter characteristics might be approached is shown in Fig. 2. Here, cavities resonating in conventional standing-wave modes are used to couple a four-port network, but difficulties in tuning this circuit are obvious. Not only must both cavities be tuned simultaneously, but the phase difference between them is critical and must be maintained over the tuning range.

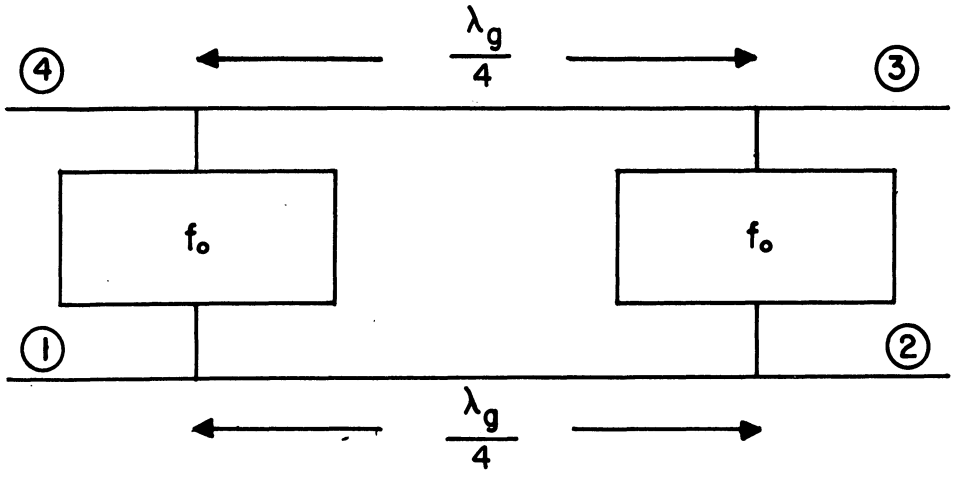

Fig. 2. A directional filter employing two resonant cavities operating in standing-wave modes.

More suitable coupling networks can be constructed using a recent innovation to resonant circuits known as a traveling-wave resonator. Using this component and ideal directional couplers, as shown in Fig. 3, one obtains a novel circuit known as a traveling-wave directional filter (Refs. 5, 6, 7), whose properties will be shown to satisfy the conditions outlined in Fig. 1. In the notation of Fig. 3, where the power coupling

factors of the individual directional couplers are denoted by $\sin^2\theta_1$ and $\sin^2\theta_2$, the scattering matrices for the ideal directional couplers are:

$$\begin{bmatrix} S_{11} & S_{12} & S_{11'} & S_{12'} \\ S_{21} & S_{22} & S_{21'} & S_{22'} \\ S_{1'1} & S_{1'2} & S_{1'1} & S_{1'2} \\ S_{2'1} & S_{2'2} & S_{2'1'} & S_{2'2'} \end{bmatrix} = \begin{bmatrix} 0 & \cos\theta_1 & 0 & j\sin\theta \\ \cos\theta_1 & 0 & j\sin\theta_1 & 0 \\ 0 & \cos\theta_1 & 0 & j\sin\theta_1 \\ \cos\theta_1 & 0 & j\sin\theta_1 & 0 \end{bmatrix} \quad (3a)$$

$$\begin{bmatrix} S_{33} & S_{34} & S_{33'} & S_{34'} \\ S_{43} & S_{44} & S_{43'} & S_{44'} \\ S_{3'3} & S_{3'4} & S_{4'3'} & S_{3'4'} \\ S_{4'3} & S_{4'4} & S_{4'3} & S_{4'4'} \end{bmatrix} = \begin{bmatrix} 0 & \cos\theta_2 & 0 & j\sin\theta_2 \\ \cos\theta_2 & 0 & j\sin\theta_2 & 0 \\ 0 & \cos\theta_2 & 0 & j\sin\theta_2 \\ \cos\theta_2 & 0 & j\sin\theta_2 & 0 \end{bmatrix} \quad (3b)$$

If $a_2 = a_3 = a_4 = 0$ in Fig. 3, then

$$b_{2'} = a_{1'}\cos\theta_1 + ja_1\sin\theta_1 \quad (4a)$$

$$b_2 = ja_{1'}\sin\theta_1 + a_1\cos\theta_1 \quad (4b)$$

$$b_3 = ja_{4'}\sin\theta_2;\ b_{3'} = a_{4'}\cos\theta_2 \quad (4c)$$

$$a_{4'} = e^{-\varphi_1}b_{2'};\ a_{1'} = e^{-\varphi_2}b_{3'} \quad (4d)$$

where $\varphi_p = (\alpha + j\beta)L_p$ $(p = 1, 2)$, and α and β represent the attenuation and the phase parameters, respectively, which are real. Resonance corresponds to $\beta(L_1 + L_2) = \beta_m L = 2m\pi$ (m = positive integer). For the present, only traveling waves in the counter-clockwise direction are considered, but if the resonator is loaded with a nonreciprocal medium, the dependence of α and β upon frequency will differ for clockwise propagation.

Eliminating $a_{1'}$, $b_{2'}$, $b_{3'}$, and $a_{4'}$ from Eqs. 4 yields the following scattering matrix coefficients for the total filter:

$$S_{31} = \frac{b_3}{a_1} = \frac{-e^{-\varphi_1} \sin\theta_1 \sin\theta_2}{1 - e^{-\varphi} \cos\theta_1 \cos\theta_2} \tag{5a}$$

$$S_{21} = \frac{b_2}{a_1} = \cos\theta_1 - \frac{e^{-\varphi} \cos\theta_2 \sin^2\theta_1}{1 - e^{-\varphi} \cos\theta_1 \cos\theta_2} \tag{5b}$$

where $\varphi = \varphi_1 + \varphi_2$. For $\alpha = 0$ (i.e., a lossless resonator) and for $\sin\theta_1 = \sin\theta_2 = \sin\theta$, Eqs. 5a and 5b have the form required by Eq. 1 and Fig. 1, so that $F(f - f_o)$ becomes

$$F\left[(\beta - \beta_m)L\right] = \frac{\sin^4\theta}{2\cos^2\theta\left[1 - \cos(\beta - \beta_m)L\right] + \sin^4\theta} \tag{6}$$

Inspection of Eq. 6 shows it to be symmetrical about $\beta = \beta_m$, and to yield a fractional bandwidth approximately equal to $\sin^2\theta$ for $\sin^2\theta \ll 1$. However, it is interesting to note that $F(0) = 1$ regardless of the value of coupling (i.e., $\sin^2\theta$). Therefore, for a lossless resonator, a free choice of coupling is available to yield any desired filter bandwidth.

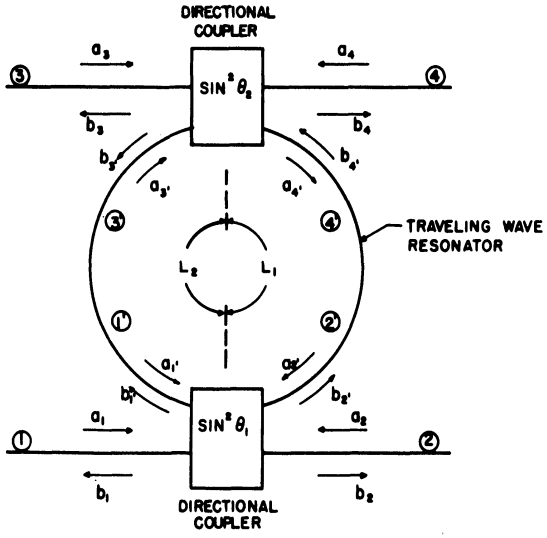

Fig. 3. A directional band-pass, band-elimination filter employing a traveling-wave resonator.

If resonator loss is considered, the ideal characteristics of Fig. 1 are best approximated by choosing

$$\frac{\cos^2\theta_2}{\cos^2\theta_2} = e^{2\alpha L} \tag{7}$$

This relation represents an optimum condition in the following sense.

If one of the coupling coefficients is specified, Eq. 7 makes S_{21} vanish at midband ($\beta = \beta_m$) and also maximizes $|S_{31}|$ at midband, such that

$$|S_{31}|^2_{max} = \frac{e^{-2\alpha L_1} \sin^2\theta_2}{\sin^2\theta_1} \tag{8}$$

It may be noted from the symmetry of Eq. 5a that S_{31} is independent of an interchange of the two directional couplers. This transposition inverts the $\sin^2\theta_2/\sin^2\theta_1$ ratio in Eq. 8 such that the numerator of Eq. 8 always contains the smaller coupling coefficient. However, perfect band rejection will not be preserved at port 2 in this case, and consequently Eq. 7 will be taken to yield optimum filter performance for given values of resonator loss.

Under the condition of Eq. 7, the bandwidth of the resonator can be shown to depend explicitly upon $\sin^2\theta_1$ (i.e., the input directional coupler), and therefore Eq. 8 has been plotted (Fig. 4) as a function of $\sin^2\theta_1$ and resonator loss. The latter is expressed in units of db per cycle, where the term cycle designates the angle $\beta_m L$. In plotting Fig. 4, L_1 has been set equal to zero, and therefore $8.68\ \alpha L_1$ db must be subtracted from the ordinate when L_1 is not zero. It is evident from Fig. 4 that filter performance is quite sensitive to resonator loss.

3. ANALYSIS OF COAXIAL TRAVELING-WAVE RESONATORS

The coaxial traveling-wave resonator shown in Fig. 5 offers sufficient generality to warrant investigation in some detail. From the traveling-wave point of view, this resonator could be looked upon as a rectangular waveguide bent into a closed loop. Such a description is misleading, however, because it disguises the connection between traveling-

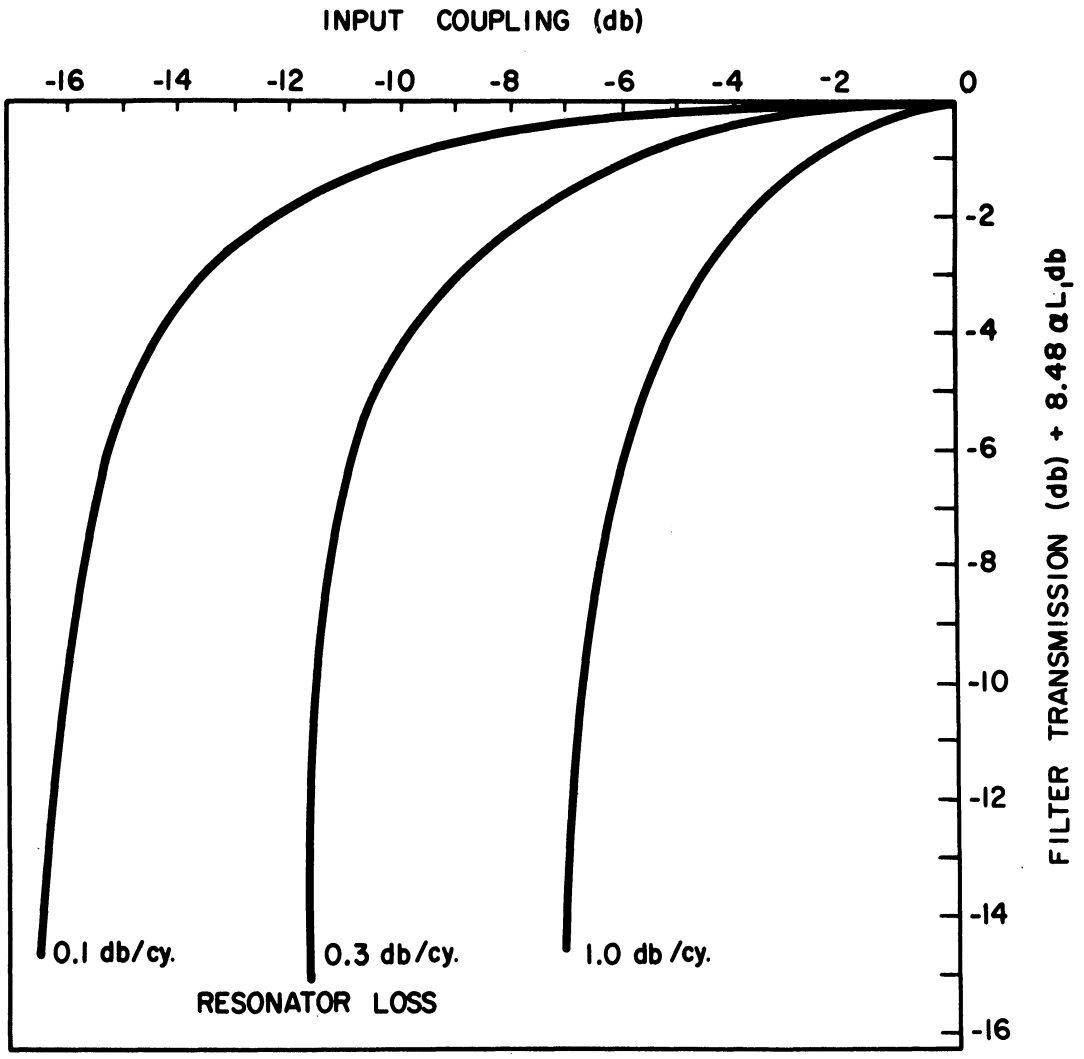

Fig. 4. Filter transmission loss in db as a function of resonator loss and input coupling.

wave modes and the conventional standing-wave modes of a coaxial cavity. In fact, it is easily shown that, corresponding to each traveling-wave mode, there is a standing-wave mode with the same resonant frequency.[1] As proof, consider the field configurations of the m, n, p coaxial-cavity modes, which can be established by exciting the cavity through an arbitrary nondirectional hole.

[1] It will be shown that the converse is not always true, since there are no traveling-wave equivalents for the TEM and $TM_{m, n, p}$ coaxial-cavity modes, when m = 0.

$$H_z = C_m(k_c r) \cos m\varphi \sin \frac{p\pi z}{h} e^{j\omega t}; \qquad TE_{m,\,n,\,p}$$

$$E_z = C_m(k_c r) \cos m\varphi \cos \frac{p\pi z}{h} e^{j\omega t}; \qquad TM_{m,\,n,\,p} \tag{9}$$

$$E_r = -\frac{1}{k_c^2}\left[\frac{p\pi}{h}\frac{\partial E_z}{\partial r} + \frac{j\omega\mu_o}{r}\frac{\partial H_z}{\partial \varphi}\right] \tag{10a}$$

$$E_\varphi = \frac{1}{k_c^2}\left[-\frac{p\pi}{hr}\frac{\partial E_z}{\partial \varphi} + j\omega\mu_o\frac{\partial H_z}{\partial r}\right] \tag{10b}$$

$$H_r = \frac{1}{k_c^2}\left[\frac{j\omega\epsilon_o}{r}\frac{\partial E_z}{\partial \varphi} - \frac{p\pi}{h}\frac{\partial H_z}{\partial r}\right] \tag{11a}$$

$$H_\varphi = \frac{1}{k_c^2}\left[j\omega\epsilon_o\frac{\partial E_z}{\partial r} + \frac{p\pi}{hr}\frac{\partial H_z}{\partial \varphi}\right] \tag{11b}$$

Here $C_m(x) = A_m J_m(x) + B_n N_m(x)$, where $J_m(x)$ and $N_m(x)$ are Bessel functions of the first and second kinds. The quantity k_c is evaluated by requiring the tangential component of E to vanish at r = a and r = b, which yields the following transcendental equations for k_c [with prime (') indicating differentiation].

$$-\frac{A_m}{B_m} = \frac{N_m(k_c a)}{J_m(k_c a)} = \frac{N_m(k_c b)}{J_m(k_c b)} \qquad TM_{m,\,n,\,p} \tag{12a}$$

$$-\frac{A_m}{B_m} = \frac{N_m'(k_c a)}{J_m'(k_c a)} = \frac{N_m'(k_c b)}{J_m'(k_c b)} \qquad TE_{m,\,n,\,p} \tag{12b}$$

The mode index n arises because these equations have an infinite number of roots in k_c. The nth-largest value of k_c corresponds to a field configuration with n half-periods in the radial direction. Similarly, the index p describes the number of half-periods in the z direction. A case of particular interest occurs when p = 0, yielding the $TM_{m,\,n,\,0}$ modes, whose resonant frequencies are the cutoff frequencies of the $TM_{m,\,n}$ coaxial-waveguide modes. In general, the resonant frequencies of all modes

are given by

$$\omega^2\mu_o\epsilon_o = k_c^2 - \left(\frac{p\pi}{h}\right)^2 \tag{13}$$

Consider now the introduction of a second signal at an angle $\pi/2m$ from the first, and out of time phase by $\pi/2$. The field configuration of this second standing-wave pattern can be determined from

$$\begin{aligned} H_z &= jC_m(k_c r)\sin m\theta \sin\frac{p\pi z}{h} e^{j\omega t} && TM_{m,\,n,\,p} \\ E_z &= jC_m(k_c r)\sin m\theta \cos\frac{p\pi z}{h} e^{j\omega t} && TE_{m,\,n,\,p} \end{aligned} \tag{14}$$

Therefore when these two inputs are present simultaneously, the resultant field configuration is given by

$$\begin{aligned} H_z &= C_m(k_c r)\sin\frac{p\pi_z}{h} e^{j(\omega t + m\varphi)} && TE_{m,\,n,\,p} \\ E_z &= C_m(k_c r)\cos\frac{p\pi_z}{h} e^{j(\omega t + m\varphi)} && TM_{m,\,n,\,p} \end{aligned} \tag{15}$$

which, for $m \neq 0$, describes a traveling wave propagating in the negative φ direction. Thus each traveling-wave mode is equivalent to two conventional standing-wave modes whose time and angular phases differ by $\pi/2$ and $\pi/2m$, respectively. Furthermore, each higher-order coaxial cavity mode ($m \neq 0$) is equivalent to the superposition of two traveling-wave modes propagating in opposite directions. It should be noted that although the latter statement resembles the conventional description of

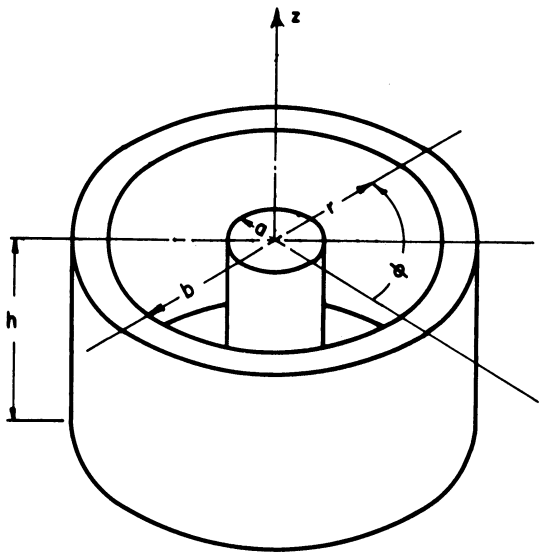

Fig. 5. A coaxial traveling-wave resonator.

a standing wave as the sum of two traveling waves, the idea of reflection is not implied. In many cavity resonators (e.g., rectangular cavities) waves propagating in only one direction cannot exist.

Returning to the original traveling-wave directional filter, it is seen that the excitation of the resonator through a directional coupler (i.e., in a traveling wave) is equivalent to exciting it through two nondirectional couplers spaced by $\pi/2m$ radians around the circumference, with signals $\pi/2$ radians out of time phase. Therefore, when a coaxial traveling-wave resonator is excited in "race track" fashion by a directional coupler (i.e., producing traveling waves in one direction only), the resonator is constrained to operating in only one of two degenerate (m, n, p) coaxial-cavity modes.

4. THE INTRODUCTION OF FERRITE INTO A TRAVELING-WAVE RESONATOR

Having established the value of the traveling-wave resonator as a filter component, it is natural to consider the introduction of ferrite for tuning this circuit. One possible technique for introducing ferrite is illustrated in Fig. 6. Here, the phase-shifting effect of the ferrite ring is related to that of an infinite ferrite slab in a straight rectangular guide (Ref. 8). Three fundamental problems immediately present themselves however. These are: (1) ferrite losses, (2) higher-order modes, and (3) the relatively high dielectric constant of ferrite materials.

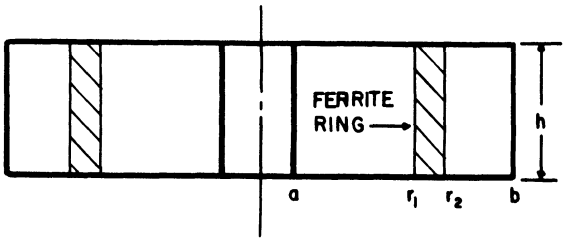

Fig. 6. A coaxial traveling wave resonator loaded with a ferrite ring.

The effect of ferrite losses is evident from the previous dis-

cussion of lossy traveling-wave directional filters. Since ferrite losses can be lumped with cavity losses, any ferrite loss will lower $|S_{13}|$ and increase its dependence on the magnitude of coupling. At the same time, the effect of higher-order modes places a practical limit on useful tuning range, if tuning is to be single-valued with respect to the applied magnetic field. From the standpoint of tuning range, it is desirable to select as the operating mode the one whose resonant frequency is the most widely separated from that of neighboring modes. Since this mode will be the fundamental, the resonator dimensions should be chosen to yield the desired frequency of the fundamental mode and a maximum frequency for the first higher mode.

The lowest-frequency traveling-wave resonator mode is the TM_{110}, whose frequency is determined by the dimensions a and b only, as are all $TM_{m, n, 0}$ modes. The first higher mode can be either TE_{110} or TM_{210}, but by choosing the cavity dimension (h) small enough, the resonant frequency of the former can be made as high as one chooses. The ratio b/a can then be chosen to yield the greatest frequency ratio of the TM_{210} mode to the TM_{110} mode; this can be shown to be 1.34 and occurs for a = 0. Thus the cavity mode offering the greatest potential tuning range is the TM_{110} cylindrical cavity mode.

In actual practice, however, the 34 percent tuning range predicted above may not be attainable because of the dielectric loading of commercially available ferrite materials, whose dielectric constant is usually 10 or greater. Although ferrite samples can generally be located where electric fields are small, the fairly large samples necessary for wideband tuning invariably introduce dielectric effects. Frequently these effects lower the resonant frequencies of higher-order modes more

rapidly than those of lower-order modes, and this further restricts the tuning range.

The question also arises as to whether higher-order modes can be suppressed by a judicious choice of coupling. Since the TM_{210} and TM_{110} modes have opposite symmetry about the cavity axis, there are several coupling techniques that can suppress the TM_{210} mode, as will be described later. However, it should be recalled that the transmission of a traveling-wave directional filter is relatively insensitive to the magnitude of coupling, and hence small imperfections in mode suppression could produce significant filter transmissions in higher-order modes. Therefore it will be assumed to be desirable to maximize the tuning range below the resonance frequency of the first higher-order mode.

5. THE CHOICE OF FERRITE LOCATION IN A TM_{110} CYLINDRICAL CAVITY

The problem of determining ferrite configurations in a cylindrical cavity that will yield a desired tuning range, with a minimum of the defects mentioned in the previous section, is necessarily complex. One reasonable simplification is the use of a ferrite ring, as in Fig. 6, since this is the only simple geometry that avoids internal reflections. With this assumption, the cavity in Fig. 6 (with a = 0) can be analyzed for the $TM_{m,\,n,\,0}$ modes as follows+

In a ferrite medium, Maxwell's equations take the form

$$\text{curl } \vec{E} = -j\omega\mu_o ||\mu|| \vec{H} \tag{16}$$

$$\text{curl } \vec{H} = j\omega\epsilon_o\epsilon_r \vec{E}$$

where $||\mu||$ is the familiar Polder permeability tensor, and is based on the approximation that ferrite behaves as a gyromagnetic medium. Choosing

a cylindrical coordinate system and a dc magnetic field H_0 applied in the +z direction (and $e^{j\omega t}$ time dependence), $||\mu||$ relates the RF components of magnetic induction and magnetic field in the following way:

$$\begin{bmatrix} B_r \\ B_\varphi \\ B_z \end{bmatrix}_{(RF)} = \begin{Vmatrix} \mu & -j\nu & 0 \\ j\nu & \mu & 0 \\ 0 & 0 & 1 \end{Vmatrix} \begin{bmatrix} H_r \\ H_\varphi \\ H_z \end{bmatrix}_{(RF)} \tag{17}$$

Here, μ and ν are well-known complex functions of both frequency and dc H_0 (see Ref. 8 for example).

Consider now the case of a traveling wave in the cylindrical resonator of Fig. 6, where $E_r = E_\varphi = H_z = 0$ throughout the cavity for $TM_{m,\,n,\,0}$ modes. Assuming a lossy ferrite medium the φ dependence is taken as $e^{-j\gamma\varphi}$, where $\gamma = \pm m + j\alpha$, and the + and - correspond to traveling waves in the $+\varphi$ and $-\varphi$ directions, respectively. Equations 16 then yield,

$$H_\varphi = \frac{1}{j\omega\mu_0\mu_e}\left[\frac{\partial E_z}{\partial r} + \frac{\gamma\psi E_z}{r}\right] \tag{18}$$

$$H_r = \frac{1}{\omega\mu_0\mu_e}\left[\psi\frac{\partial E_z}{\partial r} + \frac{\gamma E_z}{r}\right] \tag{19}$$

$$\frac{1}{r}\frac{\partial}{\partial r}\left[\frac{r\partial E_z}{\partial r}\right] + \left[k_f^2 - \frac{\gamma^2}{r^2}\right]E_z = 0 \tag{20}$$

where

$$\mu_e = \frac{\mu^2 - \nu^2}{\mu} \qquad \psi = \frac{\nu}{\mu} \tag{21}$$

$$k_f^2 = \mu_e\epsilon_r k_a^2 \qquad k_a^2 = \omega^2\mu_0\epsilon_0$$

Since Eq. 20 is Bessel's equation of order γ, E_z can be written[1]

[1] Since $k_f = \sqrt{\epsilon_r\mu_e}k_a$, and since the real part of μ_e becomes negative for moderate values of H_0, a convenient form for Eq. 22, when $\mu_e < 0$, is $E_z = A_\gamma\,[I_\gamma(-jk_fr) + B_\gamma K_\gamma(-jk_fr)]$, where I_γ and K_γ are modified Bessel functions of the first and second kinds. The subsequent equations can be similarly modified.

$$E_z = A_\gamma [j_\gamma(k_f r) + B_\gamma N_\gamma(k_f r)]$$
$$= A_\gamma X_\gamma(k_f r) \tag{22}$$

Therefore Eqs. 18 and 19 yield

$$H_\varphi = \frac{k_f}{j\omega\mu_o\mu_e} \left[X'_\gamma (k_f r) + \frac{\gamma\psi}{k_f r} X_\gamma(kr)\right] \tag{23}$$

$$H_r = \frac{k_f}{\omega\mu_o\mu_e} \left[\psi X'_\gamma (k_f r) + \frac{\gamma}{k_f r} X_2(k_f r)\right] \tag{24}$$

Equations 22, 23, and 24 are also valid in the air-filled regions of the cavity with $\mu_e\epsilon_r = 1$, $k_a = k_f$, and $\psi = 0$. Therefore, for $0 \leq r < r_1$, $B_\gamma = 0$ in Eq. 22; while for $r_2 < r \leq b$,

$$E_z = C_\gamma [J_\gamma(k_z r)\, N_\gamma(k_a b) - J_\gamma(k_a b)\, N_\gamma(k_a r)]$$
$$= C_\gamma Z_\gamma(k_a r) \tag{25}$$

since $E_z = 0$ at $r = b$.

Therefore, the total field configuration in Fig. 6 is as follows.

$$E_z = J_\gamma(k_a r) \qquad j\omega\mu_o H_\varphi = k_a J'_r(k_a r) \qquad 0 \leq r < r_1$$

$$= A_\gamma X_\gamma(k_f r) \qquad = \frac{k_f A_\gamma}{\mu_e} \left[X'_\gamma (k_f r) + \frac{\psi\gamma}{k_f r} X_\gamma(k_f r)\right] \qquad r_1 < r < r_2 \tag{25}$$

$$= C_\gamma Z_\gamma(k_a r) \qquad = k_a C_\gamma Z'_\gamma (k_a r) \qquad r_2 < r < b$$

Applying the boundary conditions that E_z and H_φ be continuous at $r = r_1$ and $r = r_2$ yields,

$$\frac{(k_a r_1) J'_\gamma(k_a r_1)}{J_\gamma(k_a r_1)} = \frac{1}{\mu_e} \left[\frac{(k_f r_1)\, X'_\gamma(k_f r_1)}{X_\gamma(k_f r_1)} + \gamma\psi\right] \tag{26}$$

$$\frac{(k_a r_2) Z'_\gamma(k_a r_2)}{Z_\gamma(k_a r_2)} = \frac{1}{\mu_e} \left[\frac{(k_f r_2)\, X'_\gamma(k_f r_2)}{X_r(k_f r_2)} + \gamma\psi\right] \tag{27}$$

In principle, Eqs. 26 and 27 are exact solutions that will give

the resonance frequency and attenuation for each value of H and for arbitrary r_1 and r_2 in the range (0, b). Since this calculation is very tedious, even if loss is neglected, a complete solution has not been made. However, considerable information can still be obtained by applying these equations to certain special cases.

Two cases of particular interest are (1) $r_1 = 0$, and (2) $r_2 = b$, which place a ferrite post or a ferrite ring, respectively, in regions of strong magnetic fields and weak electric fields. It is further assumed that loss is neglected, so $\gamma = \pm m$. Note that whenever $\pm$ signs appear henceforth the upper sign corresponds to propagation in the $+\theta$ direction.

For case (1); $B_m = 0$, Eq. 26 can be dropped, and Eq. 27 can be expanded as follows:

$$\frac{(k_a r_2)\, J'_m(k_a r_2)}{J_m(k_a r_2)} + \frac{2J_m(k_a b)}{\pi J_m(k_a r_2)[J_m(k_a b)\, N_m(k_a r_2) - J_m(k_a r_2)\, N_m(k_a b)]} = \frac{1}{\mu_e}\left[\frac{(k_f r_2)\, J'_m(k_f r_2)}{J_r(k_f r_2)} \pm m\psi\right] \tag{28}$$

Similarly, for case (2); Eq. 27 can be dropped, $B_m = -J_m(k_f b)/N_m(k_f b)$, and Eq. 26 can be written:

$$\frac{(k_a r_1)\, J'_m(k_f r_k)}{J_m(k_a r_1)} = \frac{1}{\mu_e}\left[\frac{(k_f r_2)\, J'_m(k_f r_2)}{J_m(k_f r_1)} + \frac{2J_m(k_f b)}{\pi J_m(k_f r_2)[J_m(k_f b)\, N_m(k_f r_2) - J_m(k_f r_2) N_m(k_f b)} + m\psi\right] \tag{29}$$

Although a complete analysis of these equations would still be lengthy, considerable information can be obtained from the special cases where $\psi = 0$ and $\mu_e = 0$. The former occurs when $H_0 = 0$, and the latter when $H_0 = H_{0_r} - M_0$, where H_{0_r} is the dc magnetic field corresponding to ferromagnetic resonance and M_0 is the saturation magnetization of the ferrite. If it is assumed that $\mu_e = 0$ marks the threshold of excessive loss in the ferrite, then the solutions of Eqs. 28 and 29 for $\psi = 0$ and $\mu_e = 0$ can be taken as the practical bounds on useful tuning range. Admittedly, this is an arbitrary choice, but since it is mathematically

expedient this criterion will be given further consideration. It can be noted, when tuning is very sensitive to H_0, that H_{0_r} will be considerably greater than M_0, and hence μ_e may vanish considerably before excessive loss begins. In this case, the tuning range assumed above will be conservative. On the other hand, if tuning is not very sensitive to H_0, $\mu_e = 0$ is a reasonable threshold. Therefore, it seems reasonable to interpret this tuning criterion as yielding a practical lower bound on tuning range.

The evaluation of Eqs. 28 and 29 for $\psi = 0$ (i.e., $H_0 = 0$) is straightforward and has been done for b = 0.75 inch, $\epsilon_r = 12$, $\mu = 0.7$, and m = 1, 2. The choice of $\mu = 0.7$ for $H_0 = 0$ is based on experimental data, since the tensor permeability in Eq. 17 is assumed to apply above magnetic saturation only. The results in this case are plotted in Fig. 7, which shows the resonance frequencies of the TM_{110} and TM_{210} modes vs. r_1 and r_2 (i.e., the post and ring radius, respectively) when the ferrite is unmagnetized. For $\mu_e = 0$, only the case m = 1 is of interest and Eqs. 28 and 29 simplify as follows. Below ferromagnetic resonance, $\mu_e \rightarrow 0$ corresponds to $(\mu - \nu) \rightarrow 0$ in the Polder tensor. Therefore, for μ_e nearly zero, the right-hand side of Eq. 28 behaves as

$$\frac{1}{\mu \pm \nu} \tag{30}$$

while the right-hand side of Eq. 29 varies as

$$\frac{1}{\mu \pm \nu} + \frac{1}{\mu_e}\left(\frac{2b^2}{r_2^2 - b^2}\right) \tag{31}$$

It is apparent that Eq. 30 approaches infinity for propagation in the $+\theta$ direction and $1/2\mu$ for $-\theta$ propagation, while Eq. 31 approaches infinity for either direction of propagation. Therefore, for $\mu_e = 0$, Eq. 28 reduces to

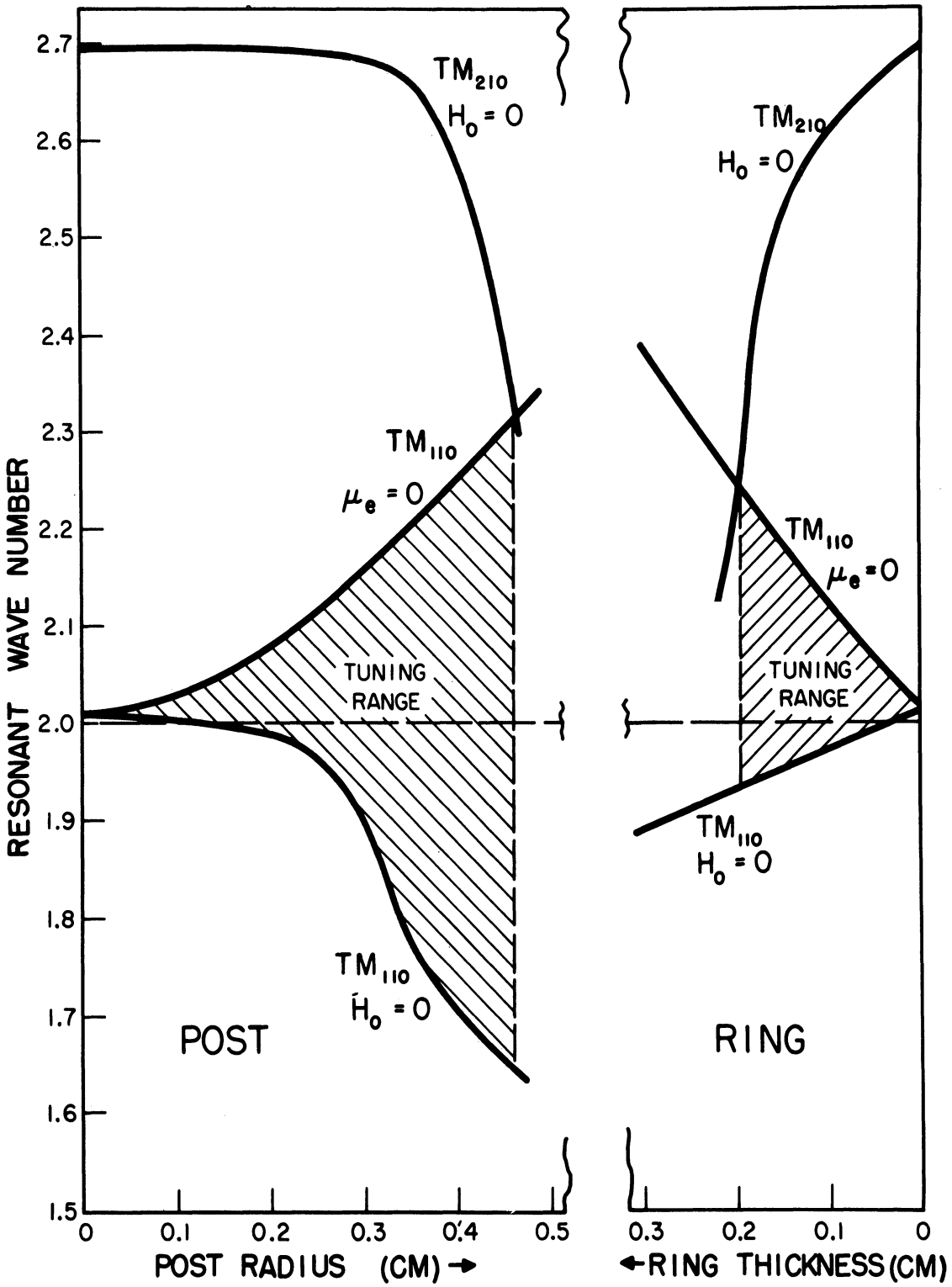

Fig. 7. Minimum tuning ranges for ferrite rings and posts as predicted by tuning criteria adopted in text.

$$\frac{J_1(k_a b)}{J_1(k_a r_2)} = \frac{N_1(k_a b)}{N_1(k_a r_2)} \tag{32}$$

for the post with $+\theta$ propagation, and Eq. 29 reduces to

$$J_1(k_a r_2) = 0 \tag{33}$$

for the ring with either $+\theta$ or $-\theta$ propagation. The solutions shown by Eqs. 32 and 33 are also shown in Fig. 7.

Comparison of Eqs. 32 and 33 with Eq. 12a shows, when $\mu_e = 0$, that the resonance frequency of the post with $+\theta$ propagation is identical to that of a coaxial cavity with radii r_2 and b, while the resonance frequency of the ring is identical to that of a cylindrical cavity with radius r_2. Thus, in each of these cases, the ferrite appears as a perfect conductor when $\mu_e = 0$ (which is a generally quoted ferrite property), except in the case of the ferrite post with $-\theta$ propagation. This result suggests that when $\mu_e = 0$, a ferrite acts like a conductor to a linearly-polarized wave (as is presented to the ring) or to a positive circularly-polarized wave (as is presented to the post with $+\theta$ propagation), but that it does not act like a conductor to a negative circularly-polarized wave.

Since μ_e is a monotonically decreasing function of H (below ferromagnetic resonance), tuning is expected to increase monotonically with H for any case where the ferrite behaves as a conductor at $\mu_e = 0$. Both experimental evidence and numerical solution of Eqs. 28 and 29 substantiate this statement. In the case of a ferrite post with $-\theta$ propagation, tuning is still observed, but it is not monotonic. This fact generally makes the $-\theta$ mode less desirable for tuning, but it can be used to extend the tuning range of the $+\theta$ mode if H_0 is varied over both negative and positive values, since the $+\theta$ mode resembles the $-\theta$

mode when H_0 is reversed. This technique is somewhat undesirable, however, since ferrite losses tend to be high for H_0 near zero (i.e., below saturation). Also, the dependence of resonance frequency upon H_0 is extremely nonlinear near saturation. Therefore, only tuning with positive H_0 will be considered further.

By returning now to Fig. 7, the approximate tuning ranges of the post and ring configurations can be compared. This figure demonstrates that a post thickness of 0.46 cm can be tolerated before the TM_{210} mode appears in the tuning band, and this thickness provides a tuning range of greater than 30 percent. In the case of the ring configuration, however, the TM_{210} mode enters the tuning range at a thickness of 0.2 cm and thereby limits the tuning range to about 16 percent. This suggests that the post configuration is preferable from the point of view of maximum tuning range.

If one now considers ferrite losses, the question arises as to which configuration will yield the smaller insertion loss for a given tuning range. The exact evaluation of insertion loss in each of these cases is tedious, so it is expedient to assume that it is proportional to ferrite thickness, at least for small thicknesses. Some support for this assumption can be gained from Fig. 7, where it can be seen that tuning range is proportional to thickness for thin posts or rings. An analogy can then be drawn with other nonlinear reactive materials (e.g., ferroelectrics and variable capacitance diodes) where insertion loss is approximately proportional to tuning range. On the basis of this assumption, Fig. 7 suggests that the ring geometry is preferable from the point of view of minimizing midband insertion loss from terminals 1 to 3 in Fig. 3. For example, a ring thickness of 0.2 cm yields the maxi-

mum useful range of 16 percent, while a post of 0.2 cm radius yields only 8 percent tuning range.

6. EXPERIMENTAL RESULTS

In view of the larger tuning rates predicted above for thin ferrite rings vs. thin ferrite posts, an experimental study of ferrite rings on the outer wall of a coaxial cavity was carried out. Attempts were made to develop a cavity with a 20 percent tuning for the TM_{110} mode, and with a minimum insertion loss envelope over this band.

Two ways of exciting a TM_{110} traveling-wave mode have been considered. The first is with 3-decibel directional couplers, which are used to provide a $\pi/2$ phase shift between two input lines and between two output lines, all spaced by 90° around the cavity (Ref. 4). This configuration is shown in Fig. 8. The second method is to excite the cavity by a circularly-polarized field rotating about the axis of the cavity (Ref. 3) as shown in Fig. 9. In both cases, the symmetry of the exciting fields is such that the TM_{210} mode should be suppressed. In Fig. 9, the coupling holes have been placed over the position of circular polarization in the input and output waveguides.

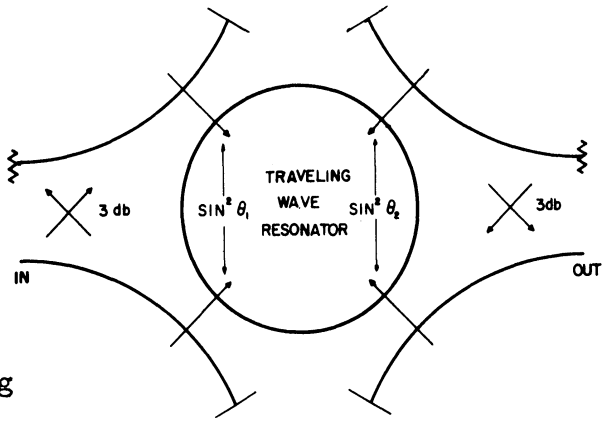

Fig. 8. A traveling-wave directional filter employing 3-db directional couplers.

Although this position is frequency sensitive, it was decided to employ the latter coupling technique first, with the additional plan of attempting to broadband the coupling at a later date, following the procedure

of Cohn (Ref. 9). In view of this plan, the waveguides were so attached that the coupling holes could be moved during the experiment. It was felt that this would allow each part of the tuning band to be measured with holes of optimum directivity. In the experiments conducted, however, the ferrite losses were of such a magnitude that large coupling holes were necessary to avoid excessive insertion losses. When the coupling holes were large, their directivity appeared to be uniformly poor with frequency, and the coupling hole positions for minimum insertion loss varied very little with frequency over the tuning band.

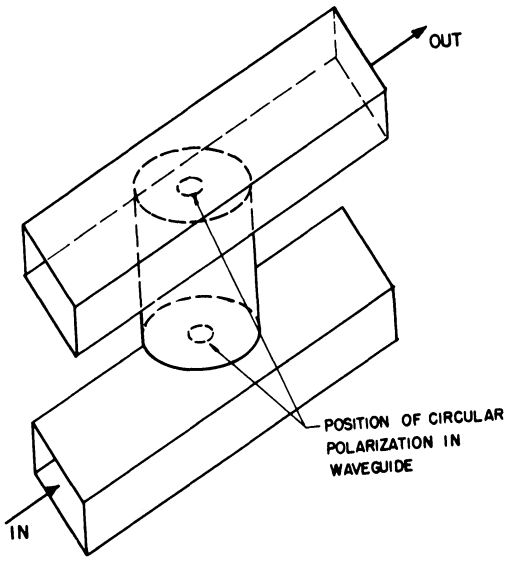

Fig. 9. A traveling-wave directional filter employing directional coupling holes.

A typical experimental result for the filter shown in Fig. 9, and loaded with a ferrite ring on the outer cavity wall, is shown in Fig. 10. These data were obtained with a 1.54" OD cavity that was loaded with a 1.50" ID, TT-390 ferrite ring. The input and output coupling holes were 7/16" and 3/8" in diameter, respectively, and were centered in the top and bottom walls of the cavity. This filter had an insertion loss of less than 10 decibels from 8.4 kmc to 10.4 kmc, but the TM_{210} mode appeared at 10.1 kmc, which limited the useful tuning range to 8.4 kmc to 10.1 kmc in this case. It will be noted that relatively poor suppression of the TM_{210} mode occurred in this case, which again points to imperfections in the coupling holes. Considerable effort

was expended to reduce the insertion loss envelope and to obtain better suppression of the TM_{210} mode, but since these two requirements conflict, little progress was made over that shown in Fig. 10.

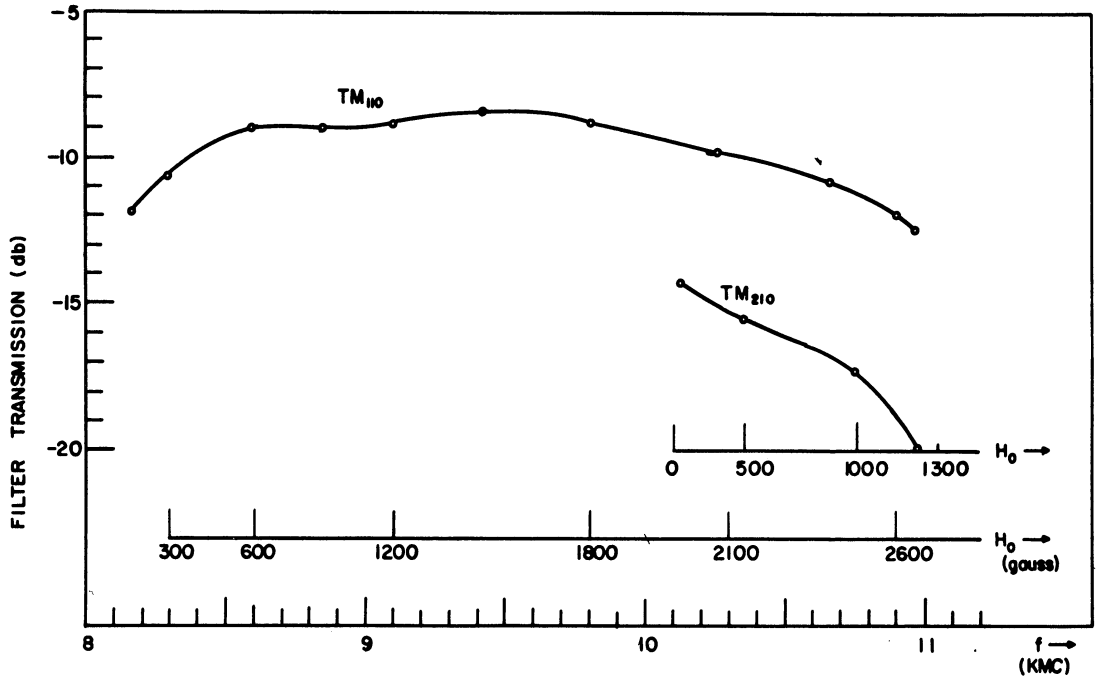

Fig. 10. A typical experimental insertion loss envelope for a wideband, ferrite-tunable, traveling-wave directional filter. Filter bandwidth approximately 5 Mc.

At the time the measurements described above were being made on the ring configuration, results were published by Whirry and Nelson (Ref. 4) on the ferrite-post configuration. They reported a tuning range of about 5 percent and an insertion loss of less than 2 decibels. Comparison of their work with work at this laboratory (CEL) supports the previous assumption that tuning range and insertion loss are roughly proportional for a given tuning medium, since the larger insertion losses measured in the CEL filters did accompany tuning ranges of 20 percent or more. However, a more qualitative comparison of these two methods would have required the fabrication of a thinner ferrite ring. Such a compari-

son was not made because of the expense of machining extra ferrite rings.

7. CONCLUSION

The usefulness of traveling-wave resonators in matched filters has been demonstrated, although the experimental development of a ferrite tunable matched filter was only partially successful. A new mode of attack would be to try ferrite geometries different from those described here, since the latter were motivated in part by ferrite phase-shifter techniques that had been demonstrated prior to 1958. More recently, a new ferrite phase-shifter principle has been discovered by Reggia and Spencer (Ref. 10), which offers strong phase shifts and low insertion losses below ferrite saturation. This phase shifter operates with a ferrite sample (a rod or slab) centered in a waveguide and magnetized in the longitudinal direction.

One technique for employing this phase shifting principle in a traveling-wave directional filter is suggested in Fig. 11. The Reggia-Spencer phase shifter has an additional advantage of requiring relatively small tuning fields, which would facilitate rapid tuning. However, this proposed filter has not been constructed, because it appears to call for considerable "cut and try" development procedures, which the author feels to be generally unjustifiable in University research.

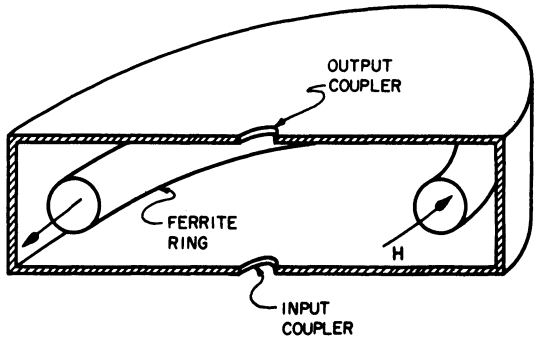

Fig. 11. Proposed technique for improving traveling-wave directional filter performance.

REFERENCES

1. G. R. Jones, J. C. Cacheris, and C. A. Morrison, "Magnetic Tuning of Resonant Cavities and Wideband Frequency Modulation of Klystrons," Proc. IRE, Vol. 44, No. 10, October 1956, pp. 1431-1438.

2. C. E. Fay, "Ferrite-Tuned Resonant Cavities," Proc. IRE, Vol. 44, No. 10, October 1956, pp. 1446-1448.

3. C. E. Nelson, "Ferrite-Tunable Microwave Cavities and the Introduction of a New Reflectionless, Tunable Microwave Filter," Proc. IRE, Vol. 44, No. 10, October 1956, pp. 1449-1455.

4. W. L. Whirry and C. E. Nelson, "Ferrite Loaded, Circularly Polarized Microwave Cavity Filters," Trans. IRE, Vol. MTT-6, No. 1, January 1958, pp. 59-65.

5. F. S. Coale, "A Traveling-Wave Directional Filter," Trans. IRE, Vol. MTT-5, October 1956, pp. 256-260.

6. S. B. Cohn and F. S. Coale, "Directional Channel-Separation Filters," Proc. IRE, Vol. 44, August 1956, pp. 1018-1024; also 1956 IRE Convention Record, Pt. 5, pp. 106-112.

7. C. E. Nelson, "Circularly Polarized Microwave Cavity Filters," Trans. IRE, Vol. MTT-5, April 1957, pp. 136-147.

8. B. Lax, K. J. Button, and L. M. Roth, "Ferrite Phase Shifters in Rectangular Waveguides," J. Appl. Physics, Vol. 25, November 1954, pp. 1413-1421.

9. S. B. Cohn, "Impedance Measurement by Means of a Broad-Band Circularly Polarized Coupler," Proc. IRE, Vol. 42, October 1954, pp. 1554-1558.

10. F. Reggia and E. G. Spencer, "A New Technique of Ferrite Phase Shifting for Beam Scanning of Microwave Antennas," Proc. IRE, Vol. 45, November 1957, pp. 1510-1516.

DISTRIBUTION LIST

Copy No.	
1-2	Commanding Officer, U. S. Army Signal Research and Development Laboratory, Fort Monmouth, New Jersey, ATTN: Senior Scientist, Countermeasures Division
3	Commanding General, U. S. Army Electronic Proving Ground, Fort Huachuca, Arizona, ATTN: Director, Electronic Warfare Dept.
4	Chief, Research and Development Division, Office of the Chief Signal Officer, Department of the Army, Washington 25, D. C., ATTN: SIGEB
5	Commanding Officer, Signal Corps Electronic Research Unit, 9560th USASRU, P. O. Box 205, Mountain View, California
6	U. S. Atomic Energy Commission, 1901 Constitution Avenue, N.W., Washington 25, D. C., ATTN: Chief Librarian
7	Director, Central Intelligence Agency, 2430 E Street, N.W., Washington 25, D.C., ATTN: OCD
8	Signal Corps Liaison Officer, Lincoln Laboratory, Box 73, Lexington 73, Massachusetts, ATTN: Col. Clinton W. Janes
9-18	Commander, Armed Services Technical Information Agency, Arlington Hall Station, Arlington 12, Virginia
19	Commander, Air Research and Development Command, Andrews Air Force Base, Washington 25, D. C., ATTN: SCRC, Hq.
20	Directorate of Research and Development, USAF, Washington 25, D. C., ATTN: Chief, Electronic Division
21-22	Hqs., Aeronautical System Division, Air Force Command, Wright Patterson Air Force Base, Ohio, ATTN: WWAD
23	Hqs., Aeronautical System Division, Air Force Command, Wright Patterson Air Force Base, Ohio, ATTN: WCLGL-7
24	Hqs., Aeronautical System Division, Air Force Command, Wright Patterson Air Force Base, Ohio - For retransmittal to - Packard Bell Electronics, P. O. Box 337, Newbury Park, California
25	Commander, Air Force Cambridge Research Center, L. G. Hanscom Field, Bedford, Massachusetts, ATTN: CROTLR-2
26-27	Commander, Rome Air Development Center, Griffiss Air Force Base, New York, ATTN: RCSSLD - For retransmittal to Ohio State University Research Foundation
28	Commander, Air Proving Ground Center, ATTN: Adj/Technical Report Branch, Eglin Air Force Base, Florida
29	Commander, Special Weapons Center, Kirtland Air Force Base, Albuquerque, New Mexico
30	Chief, Bureau of Naval Weapons, Code RRR-E, Department of the Navy, Washington 25, D. C.
31	Chief of Naval Operations, EW Systems Branch, OP-35, Department of the Navy, Washington 25, D. C.
32	Chief, Bureau of Ships, Code 691C, Department of the Navy, Washington 25, D. C.
33	Chief, Bureau of Ships, Code 684, Department of the Navy, Washington 25, D. C.
34	Chief, Bureau of Naval Weapons, Code RAAV-33, Department of the Navy, Washington 25, D. C.
35	Commander, Naval Ordnance Test Station, Inyokern, China Lake, California, ATTN: Test Director - Code 30
36	Director, Naval Research Laboratory, Countermeasures Branch, Code 5430, Washington 25, D. C.
37	Director, Naval Research Laboratory, Washington 25, D. C., Attn: Code 2021
38	Director, Air University Library, Maxwell Air Force Base, Alabama, ATTN: CR-4987
39	Commanding Officer - Director, U. S. Naval Electronic Laboratory, San Diego 52, California
40	Office of the Chief of Ordnance, Department of the Army, Washington 25, D. C., ATTN: ORDTU
41	Chief, West Coast Office, U. S. Army Signal Research and Development Laboratory, Bldg. 6, 75 S. Grand Avenue, Pasadena 2, California
42	Commanding Officer, U. S. Naval Ordnance Laboratory, Silver Springs 19, Maryland
43-44	Chief, U. S. Army Security Agency, Arlington Hall Station, Arlington 12, Virginia, ATTN: IADEV
45	President, U. S. Army Defense Board, Hqs., Fort Bliss, Texas

DISTRIBUTION LIST (Cont.)

Copy No.	
46	President, U. S. Army Airborne and Electronics Board, Fort Bragg, North Carolina
47	U. S. Army Antiaircraft Artillery and Guided Missile School, Fort Bliss, Texas
48	Commander, USAF Security Service, San Antonio, Texas, ATTN: CLR
49	Chief, Naval Research, Department of the Navy, Washington 25, D. C., ATTN: Code 931
50	Commanding Officer, U. S. Army Security Agency, Operations Center, Fort Huachuca, Arizona
51	President, U. S. Army Security Agency Board, Arlington Hall Station, Arlington 12, Virginia
52	Operations Research Office, John Hopkins University, 6935 Arlington Road, Bethesda 14, Maryland, ATTN: U. S. Army Liaison Officer
53	The John Hopkins University, Radiation Laboratory, 1315 St. Paul Street, Baltimore 2, Maryland, ATTN: Librarian
54	Stanford Electronics Laboratories, Stanford University, Stanford, California, ATTN: Applied Electronics Laboratory Document Library
55	HRB - Singer, Inc., Science Park, State College, Pennsylvania, ATTN: R. A. Evans, Manager, Technical Information Center
56	ITT Laboratories, 500 Washington Avenue, Nutley 10, New Jersey, ATTN: Mr. L. A. DeRosa, Div. R-15 Lab.
57	Director, USAF Project Rand, via Air Force Liaison Office, The Rand Corp., 1700 Main Street, Santa Monica, Calif.
58	Stanford Electronics Laboratories, Stanford University, Stanford, California, ATTN: Dr. R. C. Cumming
59	Willow Run Laboratories, The University of Michigan, P. O. Box 2008, Ann Arbor, Michigan, ATTN: Dr. Boyd
60	Stanford Research Institute, Menlo Park, California, Attn: Dr. Cohn
61	Stanford Research Institute, Menlo Park, California, ATTN: Dr. Cohn

Copy No.	
62-63	Commanding Officer, U. S. Army Signal Missile Support Agency, White Sands Missile Range, New Mexico, ATTN: SIGWS-EW and SIGWS-FC
64	Commanding Officer, U. S. Naval Air Development Center, Johnsville, Pennsylvania, ATTN: Naval Air Development Center Library
65	Commanding Officer, U. S. Army Signal Research and Development Laboratory, Fort Monmouth, New Jersey, ATTN: U. S. Marine Corps Liaison Office, Code AO-4C
66	President, U. S. Army Signal Board, Fort Monmouth, New Jersey
67-75	Commanding Officer, U. S. Army Signal Research and Development Laboratory, Fort Monmouth, New Jersey ATTN: 1 Copy - Director of Research 1 Copy - Technical Documents Center ADT/E 1 Copy - Chief, Countermeasures Systems Branch, Countermeasures Division 1 Copy - Chief, Detection and Location Branch, Countermeasures Division 1 Copy - Chief, Jamming and Deception Branch, Countermeasures Division 1 Copy - File Unit No. 2, Mail and Records, Countermeasures Division 3 Cpys - Chief, Security Division (For retransmittal to BJSM)
76	Director, National Security Agency, Fort George G. Meade, Maryland, ATTN: TEC
77	Dr. B. F. Barton, Director, Cooley Electronics Laboratory, The University of Michigan, Ann Arbor, Michigan
78-99	Cooley Electronics Laboratory Project File, The University of Michigan, Ann Arbor, Michigan
100	Project File, The University of Michigan Office of Research Administration, Ann Arbor, Michigan

Above distribution is effected by Countermeasures Division, Surveillance Department, USASRDL, Evans Area, Belmar, New Jersey. For further information contact Mr. I. O. Myers, Senior Scientist, Telephone 59 61252.